iScience

CellPress
OPEN ACCESS

Article

Interdisciplinary analysis and optimization of digital photonic devices for meta-photonics

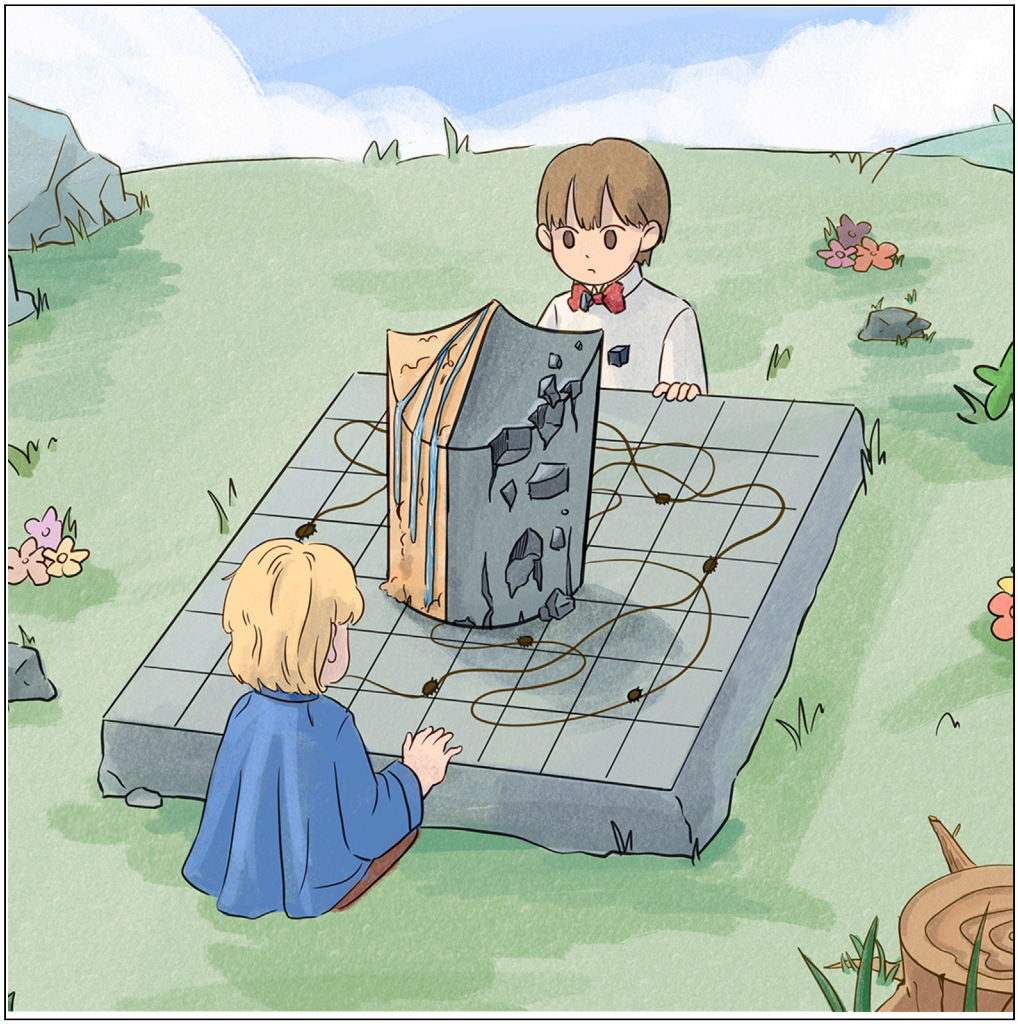

Xiaohua Xing, Yuqi Ren, Die Zou, ..., Jianquan Yao, Deyi Xiong, Liang Wu

wuliang@tju.edu.cn

Highlights

By merging knowledge from 7 domains, we explored new design schemes for optical devices

We addressed the issues by only using a 25*25 pixels metasurface structure and 54 sample data sets

Unlike previous instances of 'AI for Science', it showcases the potential for 'Science for AI'

Our work provides valuable references for AI-based design of functional devices in terahertz.

Xing et al., iScience 27, 109838
June 21, 2024
https://doi.org/10.1016/j.isci.2024.109838

iScience

CellPress
OPEN ACCESS

Article

Interdisciplinary analysis and optimization of digital photonic devices for meta-photonics

Xiaohua Xing,[1] Yuqi Ren,[2] Die Zou,[1] Qiankun Zhang,[1] Bingxuan Mao,[1] Jianquan Yao,[1] Deyi Xiong,[2] and Liang Wu[1,3,*]

SUMMARY

With the continuous integration and development of AI and natural sciences, we have been diligently exploring a computational analysis framework for digital photonic devices. Here, We have overcome the challenge of limited datasets through the use of Generative Adversarial Network networks and transfer learning, providing AI feedback that aligns with human knowledge systems. Furthermore, we have introduced knowledge from disciplines such as image denoising, multi-agent modeling of Physarum polycephalum, percolation theory, wave function collapse algorithms, and others to analyze this new design system. It represents an accomplishment unattainable within the framework of classical photonics theory and significantly improves the performance of the designed devices. Notably, we present theoretical analyses for the drastic changes in device performance and the enhancement of device robustness, which have not been reported in previous research. The proposed concept of meta-photonics transcends the conventional boundaries of disciplinary silos, demonstrating the transformative potential of interdisciplinary fusion.

INTRODUCTION

The concept of meta-photonics aims to enrich the traditional photonics system that is solely composed of monotonous physical elements, by incorporating various new approaches such as digital associations. The diverse digital association based on this approach not just enrich the knowledge system of single physical association, but also provide a new perspective for the design of photonic devices, greatly stimulating the development of the field.[1–11] Building on this design concept, we have further expanded the scope of interaction between photonics and other fields, tapping into specialized knowledge across various disciplines to present unprecedented design possibilities for devices from a fresh perspective.

In traditional photonics, achieving the target optical response has always been a crucial issue. Due to the complexity of optical response types and numerous related parameters involved, such as material, geometric parameters, and composition, any changes in these parameters would lead to completely different response effects. Therefore, in practical operations, designers usually rely solely on their personal physical experience, which faces significant limitations. Furthermore, in order to obtain the final target optical response, thousands of experiments or simulation parameter attempts are required, all of which may be just for selecting the final set of data. Once the data are selected, subsequent utilization of all data used in previous process will be minimal, and even if other researchers conduct similar research in future, they will not be able to extract any other effective data from this process. The data analyses barrier under the traditional knowledge system has brought about repetitive basic research and exploration that consume time and resources.

To better integrate, analyze, and process various data in photonic device design, and allow more data to play a certain role in photonic research, we selected small samples of unoptimized common data (including 24 narrow band-stop filters and 30 narrow band-pass filters) in our work. Each of these 54 samples, as a separate device, is not considered as an excellent functional device and is difficult to analyze or improve based on traditional photonics theory. Here, we integrated professional knowledge from seven distinct fields, including artificial intelligence, image denoising, multi-agent modeling of Physarum polycephalum, percolation theory, wave function collapse (WFC) algorithms, conventional electromagnetism, and mathematical model analysis. The primary utilization of artificial intelligence techniques is to address the issue of insufficient datasets in digitized photonics devices, enabling effective data augmentation and transfer learning. The knowledge from other disciplines aims to tackle the challenges associated with analyzing and optimizing existing digitized structural samples. This interaction method brings for the first time the possibility of secondary use of raw basic data. Additionally, it enables designing and implementing significant performance improvements for photonic devices from a new perspective, and providing original analysis and solution approaches for

[1]College of Precision Instrument and Optoelectronics Engineering, Tianjin University, Key Laboratory of Optoelectronics Information and Technology (Ministry of Education), Tianjin 300072, China
[2]College of Intelligence and Computing, Tianjin University, Tianjin 300072, China
[3]Lead contact
*Correspondence: wuliang@tju.edu.cn
https://doi.org/10.1016/j.isci.2024.109838

a series of previously unsolved problems in designs, such as the robustness of photonic device functionality to structural physical parameters, the reasons for optical property mutation under different parameters, and how to choose optimization directions when device response is inconsistent with target optical response. (In order to facilitate a better understanding of the idea and specific logical framework of this work by other readers, we have provided detailed explanations in the supplemental information.)

To demonstrate the implementation process of these different disciplines and fields and to exhibit the integration of a series of complex knowledge from various fields,[12–17] we chose a simple low-resolution (25*25) metamaterial structure, which is an aluminum square with a side length of 8 μm and a thickness of 200 nm, on a high-resistivity silicon substrate with a side length of 200 μm and a thickness of 500 μm. Through simulation and theoretical double verification of photonic devices with different types of performance obtained by combining knowledge from different fields, we have achieved expected results. This successfully demonstrates the practical feasibility of the meta-photonics. Furthermore, it shows enormous potential for the development of optical neural chips, integrated optics, image classification, optical metrology, and other fields based on this theoretical mode.[18–23] The proposed meta-photonics system, which has a diverse digital mapping relationship and contains knowledge from multiple disciplines, will certainly provide a powerful guarantee for the continuous and rapid development of the related fields, and will further lead photonic research into a new era.

RESULTS

The section that synergizes with artificial intelligence

From the inception of artificial intelligence technology to its development today, the actual performance of an intelligent system often depends on three components: data, algorithms, and computing power. Among them, algorithms and computing power are primarily constrained by the level of knowledge development and hardware technology in their respective societies. Therefore, the performance of computational models within the same period often depends on the amount of data selected for training. Similar to human learning, having ample supply of learning samples is a necessary condition for achieving excellent results. However, the integration of photonics and artificial intelligence is still in its nascent stage. Both the digital association and the effective datasets available for network learning are relatively scarce.

Thus, to verify the feasibility of the meta-photonics design pattern, we no longer rely on large datasets for the construction of deep learning networks. Instead, we utilized a Generative Adversarial Network (GAN) to generate a large number of similar pseudo-data based on small unoptimized ordinary data. GAN generates synthetic data that closely resembles the real data distribution through adversarial training between a generator network and a discriminator network. The generator takes random noise as input and generates synthetic samples in an attempt to mimic the distribution of real data. The discriminator receives both real and generated samples as input and aims to differentiate between them, classifying them as real or fake. Through the continuous games between the generator and discriminator, we obtained 3600 pseudo-data from the generator for narrowband band-pass filters and narrowband band-stop filters. Although the discriminator has difficulty in distinguishing the generated 3600 pseudo-data, we intend to select a practical application scenario to demonstrate the significance and effectiveness of these newly generated data.

We anticipate gleaning new insights into photonic device design from the vast amount of data obtained. However, the distribution of the obtained patterns is disordered. Unlike the simple shapes such as squares or circles that better conform to people's intuitive understanding, the results we have obtained are more akin to a pile of mysterious two-dimensional code. Therefore, we thought of the pre-trained Vision Transformer (ViT) model that learning rich visual representations by unsupervised learning, capturing general visual knowledge from a wide range of visual concepts. We employed a ViT model that pre-trained on ImageNet-21K dataset and fine-tuned on ImageNet-1K dataset. Although it is difficult to intuitively see the rules from these complex and varied patterns, we established a connection between the photonic device and image patterns, extracted some of the rules hidden within these unknown arrangement patterns. We utilized the ViT model for transfer learning to predict the class of photonic devices and selected a pattern with a high fitting degree and a pattern with a low fitting degree for narrowband band-pass filters and narrowband band-stop filters, respectively. For narrowband bandpass filters, the selected pattern with high fitting degree is "scabbard" and the low fitting degree is "hatchet", while for narrowband band-stop filters, the selected pattern with high fitting degree is "shield" and the low fitting degree is "analog clock". Figures 1A and 1F, respectively, show the original images selected from the ImageNet-21K, while Figures 1B–1D, and 1G-1I represent the corresponding metasurface structures constructed based on the transfer learning structure for different functions, where the blue part represents the metal patch and the yellow part represents none. The respective results are shown in the E and J on the right side of Figure 1, where the black solid line and blue dashed line represent the simulation results of the patterns with high fitting degree and low fitting degree, respectively. To make a performance comparison with traditional photonics design methods, we also introduced a classic rectangular structure of the same size, whose results are shown as the red dashed line. In this study, the traditional rectangular shape, serving as the control group for the "scabbard" structure, is located in the central region of the entire unit structure. Its outer dimensions are 172 μm in length and 91 μm in width. As for the control group of the "shield" structure, the traditional rectangular shape has outer dimensions of 140 μm in length and 153 μm in width. All other structures in this part are modeled based on these rectangular shapes as the outer boundary, while aligning with the style of the dataset images. For all narrow structure paths in this study, a minimum width of 1 pixel (8 μm) is maintained. In this work, the Computer Simulation Technology (CST) Studio Suite was employed for the simulation of terahertz transmission spectra. It is not difficult to see that the structure of the pattern with high fitting degree has a significantly better performance when applied to the design of photonic devices than that with low fitting degree. In addition, when compared with traditional structures in terms of bandwidth performance, the pattern results obtained based on this GAN and transfer learning demonstrates much better effectiveness. Furthermore, this design method brings us some new photonic device pattern results and

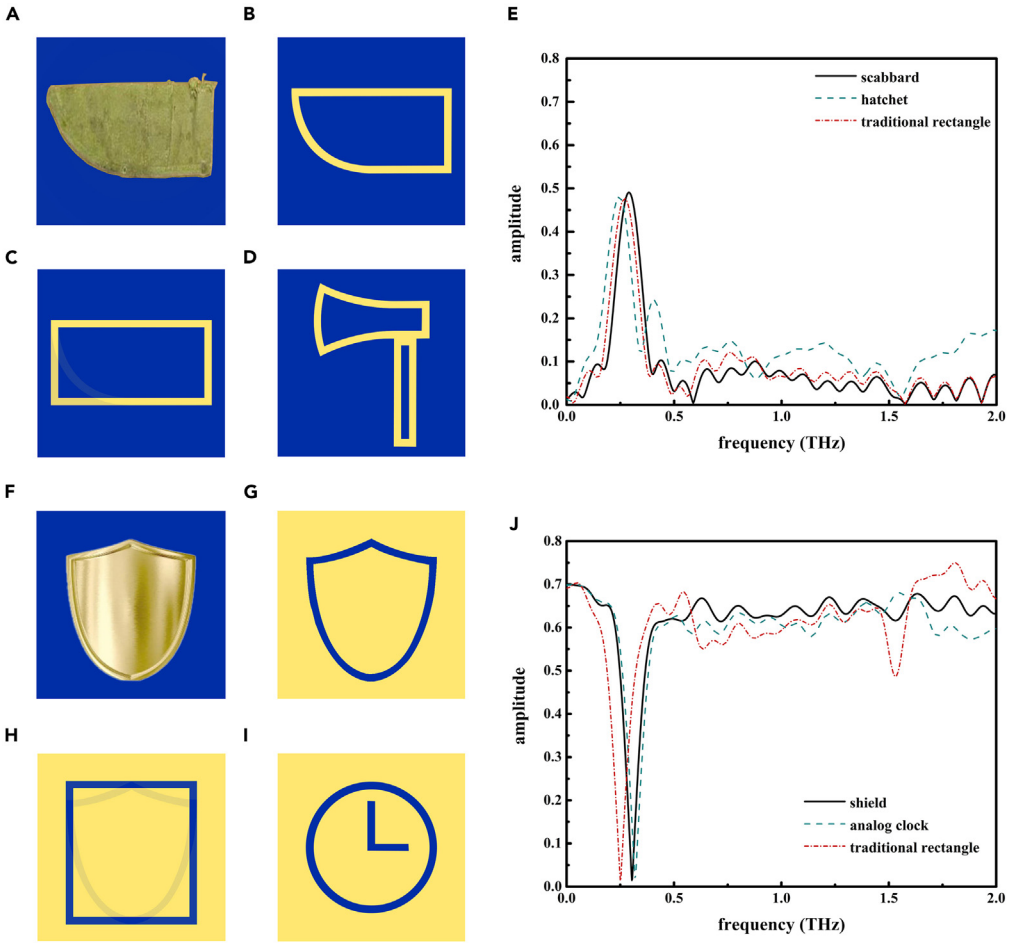

Figure 1. The results integration with artificial intelligence

(A–D), (F–I) The fitting pattern from the ViT model and the schematic of the metasurface structure designed based on the pattern.

(E) and (J) The simulation results corresponding to these structures.

design experience, such as not necessarily using straight lines or curved arcs in pattern design, namely, a mixed mode can lead to unexpected performance improvements sometimes.

The section that synergizes with conventional electromagnetism and WFC algorithms

Upon concluding our endeavor to integrate artificial intelligence with conventional photonics, let us reexamine these 54 sets of samples. Throughout the first cross-domain computation, the 25*25 "01" matrix has consistently served as one whole dataset for analysis and processing, whether in the initial photonics stage or the subsequent GAN networks and transfer learning processes. Now, by adopting a statistical perspective, we treat each "0" or "1" pixel in the 24 narrowband band-stop filters and the 30 narrowband band-pass filters as an individual with independent distribution. We hypothesize that in all samples with the same specific function, for these 625 specific positions, if the number of "1" is relatively high, then when constructing a new device with the same function or even better performance, we are more likely to choose "1" for this position. Conversely, if the number of "0"s is relatively high, we are more likely to choose "0".

We then conducted probability distribution calculations for the two distinct optical functional devices we had selected, yielding the results depicted in Figure 2. The next step is to convert this probability distribution result into a definite "01" distribution pattern on a two-dimensional plane. The critical factor in this transformation is the selection of a threshold. Based on this predetermined threshold, each structural position can be converted from an uncertain probability distribution to a definite "0" or "1" pixel.

According to conventional electromagnetism, the structural patterns for implementing band-pass and band-stop filtering using metasurfaces are often approximately complementary in geometric shape collapse in quantum mechanics. Band-pass structures typically feature geometries with gaps, akin to removing specific positions from an overall metal sheet, while band-stop structures are exactly the opposite, resembling metal patches attached to a substrate. With this consideration in mind, we determined the priority for threshold selection in this process. For the probability distribution of narrowband band-pass filters, we choose a lower threshold based on "0" pixels as much as

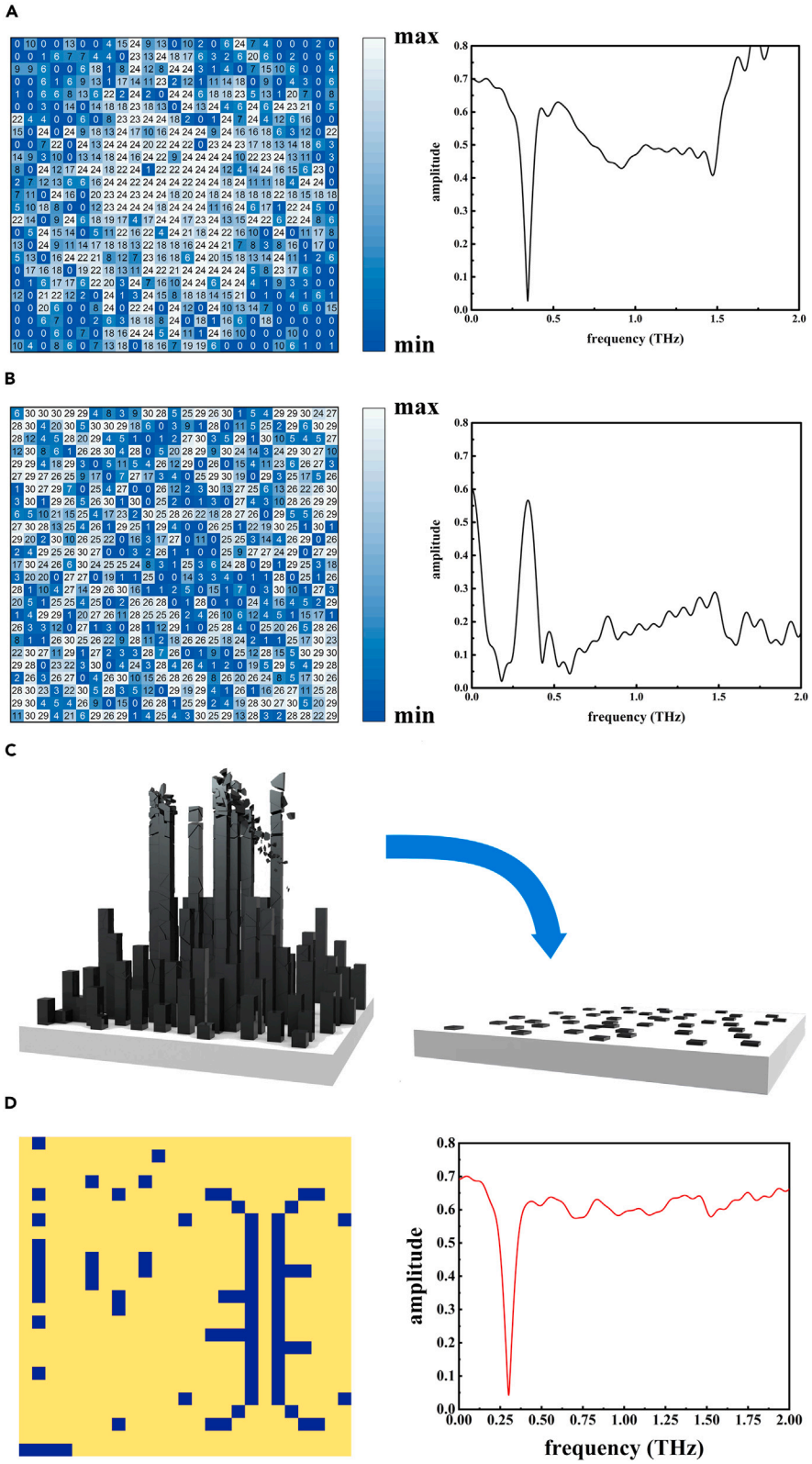
A
max
min
amplitude
frequency (THz)
B
max
min
amplitude
frequency (THz)
C
D
amplitude
frequency (THz)

Figure 2. The results integration with conventional electromagnetism and WFC algorithms

(A and B) The probability distribution schematics and simulation results for the band-stop and band-pass structures.

(C and D) The schematic of the process for designing metasurface structures based on the WFC algorithm and the simulation results.

possible to represent the "removal" process, while for the probability distribution results of narrowband band-stop filters, we choose a higher threshold based on "1" pixels as much as possible to represent the "attachment" process. Based on the optimization results, we obtained the results shown on the right side of Figure 2. Compared to single data with similar functional effects but not yet fully optimized, the data analyzed from a statistical perspective has a narrower bandwidth and improved device performance.

In addition to the simple probability distribution division based on threshold values, if we consider the entire probability distribution function as an uncertain state structure and the final selected device capable of achieving the target optical response as a definite state structure, the process from such uncertainty to certainty according to certain rules naturally reminds us of WFC in quantum mechanics.[24,25] Previous researchers have designed WFC algorithms based on this idea, primarily applied in map construction or simple games like Sudoku. This process requires two core elements: an initial definite value and a "collapse" process logic. For example, in the Sudoku game, the number given at the beginning serves as the first element, while the rule that the same number cannot appear in the same row or column is the second element. Based on this idea, we first select all the determined state numbers for each function, that is, positions where "1" or "0" is present in all data, as the first element. Due to the many theories in metasurface design that have not been precisely predicted and analyzed in complex functional devices, such as magnetic dipoles, electric dipoles, or intricate responses stemming from comprehensive effects,[26–28] we input these samples as a dataset, allowing the program to learn the potential collapse rules embedded in this type of data as completely as possible. Admittedly, this method exhibits some randomness when the sample data volume is insufficient; however, as shown in Figure 2D, we still obtained pattern distributions with superior performance compared to those based on conventional electromagnetism by scanning parameters.

The section that synergizes with mathematical model analysis and multi-agent modeling of Physarum polycephalum

In the process of constructing a metasurface based on the WFC algorithm, the selection method of the first element has provided us with an entirely new approach to solve the modeling problem. However, due to the small sample dataset used in this work, a position is considered to have a determined value only when all positions have the same value (threshold value $p = 1$), otherwise, its assignment status is considered undetermined. Combined with the structural characteristics of band-pass filters and band-stop filters mentioned in the conventional electromagnetism section, we selected the determined "0" part of the probability distribution results of the narrow-band bandpass filter and the determined "1" part of the probability distribution results of the narrow-band band-stop filter, as shown by the white dots (center points of each selected unit) in Figures 2C and S2A. In order to include these white dots in the established geometric pattern, we considered combining the way to construct polygons in mathematical model analysis to connect these white dots end to end to form the structures, where the blue part represents pixel "1" and the yellow part represents pixel "0", and their corresponding transmission spectral effects are shown in Figures S3B and S3D. Although this polygonal modeling method solves the basic requirement of encompassing all the required elements, it also introduces a new problem: the definition of redundant areas. For example, when using pixel "1" as the judgment criterion and selecting all regions with $p = 1$ to form a closed polygon, these polygons also include many regions with very small or even zero p values. These redundant areas also collectively form the final structure pattern, which will inevitably interfere with the optimization of performance to some extent.

To alleviate the issue of selection and more accurately select regions with high value of p while avoiding regions with low value of p as much as possible, we turned to Physarum.[29–31] Physarum, as a large unicellular ameba, feeds on unevenly distributed food sources through the relative continuous exploration of individuals to maximize the search of target areas, bypassing the constraints of physical barriers (it is also affected by light, and areas illuminated by light can be equivalently regarded as physical barrier areas), passing through food areas and eventually forming a tubular network. Such a path can improve the overall transport efficiency and flexibility, it has a high degree of fault tolerance for accidental disconnections. Therefore, researchers have previously used the method to plan the Tokyo railway network and practical application models such as maze solving. Inspired by this approach, some researchers also have implemented the inference of the density field of the universe from galaxy surveys. This approach finds numerous applications in scientific research and structural design.[32–37] Subsequently, based on the biological characteristics of Physarum, the multi-agent modeling of Physarum polycephalum was developed. This model combines simple particle-like intelligent agents with paracrine chemotaxis behavior in a dissipative environment, leading to the spontaneous emergence of persistent complex structures. Such artificially constructed modeling based on intelligent agents has been verified by fields that also need to simulate Physarum behavior such as astrophysics, and the results are effective and reliable.

Therefore, here we set the areas we want to select ($p = 1$) as "food" and the areas ($p = 0$) as "obstacles". By recording the paths of Physarum intelligent agents, we obtained the results shown in Figures 3A and 3C, and their respective corresponding transmission spectral results are shown in Figures 3B and 3D. It can be clearly seen that compared with the results of polygons carrying redundant areas, the structure obtained based on the multi-agent modeling of Physarum polycephalum has better effects on optimizing the target optical response performance.

This method has three significant advantages: firstly, it avoids redundant areas and more accurately selects target areas to better improve performance indicators; secondly, the paths obtained in this way are often shorter, so if the optical response effects are similar, the shorter path design means less material consumption and can effectively reduce processing costs; finally, it has outstanding structural robustness. We, respectively, tried to break paths A, B, C, and D in Figures 3A and 3C, and the optical response of this structure can maintain a high degree of stability, which is almost non-existent in traditional photonic device design. To some extent, a certain degree of damage robustness of

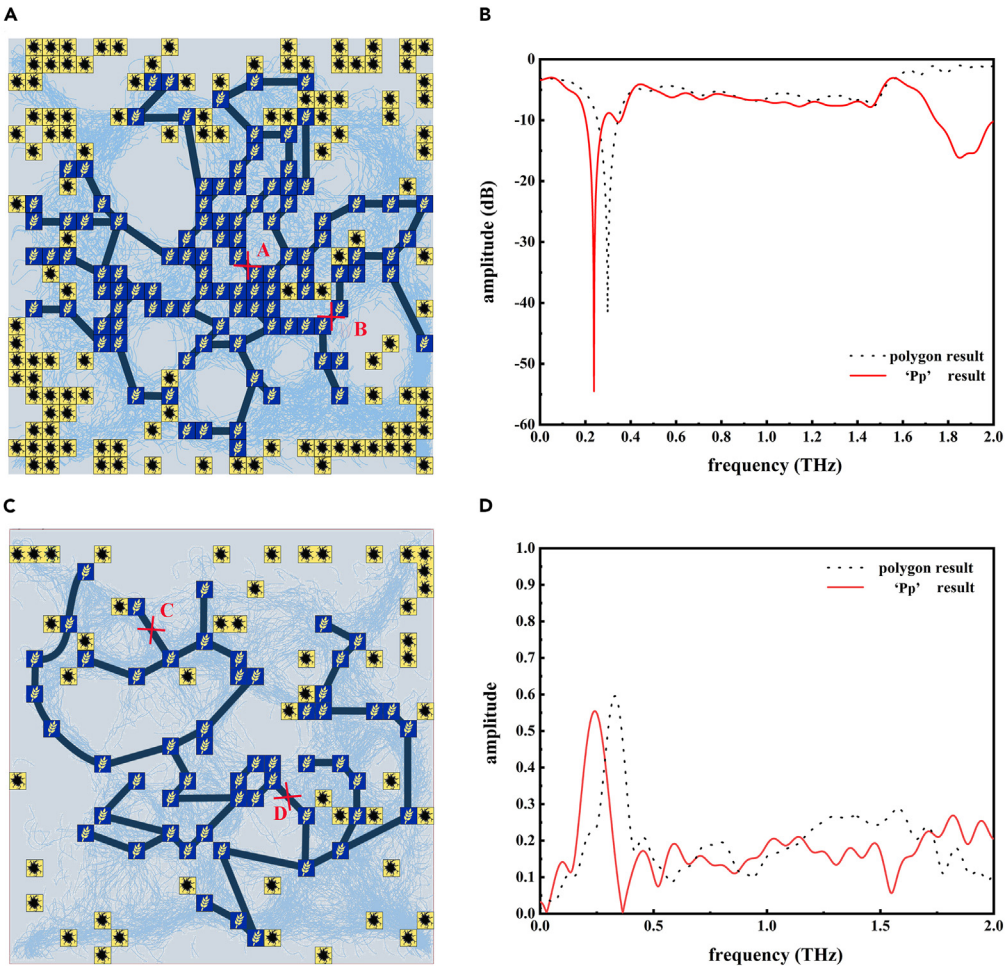

Figure 3. The results integration with multi-agent modeling of Physarum polycephalum

(A and C) The schematic of the metasurface structure with band-stop and band-pass functionalities, represented by the deep blue line path.

(B and D) The simulation results of the structure on the left, where "Pp" is the abbreviation for multi-agent modeling of Physarum polycephalum.

the device structure also provides more possibilities for photonic devices in more special critical or harsh application scenarios. In addition, if the sample size is more sufficient and the selection of the threshold probability p is more flexible, combined with Physarum algorithm and other related characterization means of Physarum behavior, more excellent design results would be waiting to be explored and discovered.

The section that synergizes with image denoising

By relying on multi-agent modeling of Physarum polycephalum, we eliminated redundant regions in structure selection. There exists a one-to-one correspondence between the physical structure of each photonic device and its selected optical response, which may be based on Finite-Difference Time-Domain (FDTD), a method that uses Maxwell's equations to divide continuous space into finite grids for analysis or based on even some yet unknown mysterious relationship. However, we acknowledge the existence of a correspondence rule, regardless of the method used. This rule is similar to the way an independent variable *x* undergoes an unknown but deterministic function f to produce a dependent variable *y*. To facilitate understanding of the subsequent analysis, we assume a mapping relationship, where "*x*" represents the metasurface structure data, "*y*" represents the corresponding transmission spectrum results, and "*f*" represents the highly nonlinear and complex relationship between the two. Based on this one-to-one correspondence, we first consider analyzing from the target optical response, "*y*", as shown in Figure S4A. We assume that the red solid line represents the expected narrowband band-stop effect, and the black solid line represents the transmission spectrum response of the current structure. By coloring the areas enclosed by these data curve separately, we obtain the image on the right. Here, we redivide this image into three distinct regions using three names: the information area, enclosed by the target spectrum data line; noise areas 1 and 2, representing the differences between the transmission spectrum and the target spectrum of the current structure based on peak positions; and the other area, which is a deep blue region with low correlation. By transforming the issue in this method, optimization of physical parameters for photonic devices is transformed into an image denoising problem, wherein

we aim to remove the noise areas as much as possible based on the existing image to improve the image quality and enhance device performance. For the metasurface structure used in this work, which comprises 25*25 pixels, different positions of pixels will have varying effects on distinct regions of the target spectrum, possibly increasing any kind of area. Although the ultimate goal is to denoise the target spectrum "*y*", we cannot directly change "*y*". Therefore, we need to utilize a similar inverse function approach, by denoising "*x*" and using the one-to-one property of the determined function "*f*", in order to complete the denoising process of "*y*". Hence, the core of removing spectral noise becomes finding which regions in the "*x*" distribution are the current selected noise of "*y*", and then performing denoising processing. Thus, we employ Gaussian filtering, a classic image denoising technique.[38–40]

Gaussian filtering, widely used for image noise reduction, is based on the central limit theorem, which states that if a random variable is the result of a large number of small, independent random factors, it generally follows a normal distribution. The common approach is to first perform a Fourier transform on the original image, then filter it, and finally perform an inverse Fourier transform to obtain the filtered image. In this work, both the "noise" and "information" in the metamaterial structure pattern distribution can be considered as the result of numerous small, independent random factors. The advantage of this approach is that although in the spatial domain pattern distribution we cannot distinguish which is noise, nor can we filter out this noise, the frequency domain result obtained by Fourier transform gives us the possibility to analyze the position of the noise. However, the nature of "noise" here may differ from the characteristics of conventional image noise after Fourier transformation in the frequency domain and requires continual attempts to transform to the selected filter parameters in the frequency domain. We utilized the NumPy library in Python to create a Gaussian filter kernel and experimented with kernel sizes of 1*1, 3*3, 5*5, 7*7, and found that the 5*5 size yielded the best results as shown in Figures S4B and S4C. We still use the probability distribution result that includes the entire sample distribution information as the original data, but this time it is an image instead of a matrix. After the same process as the classic Gaussian filtering is performed, i.e., Fourier transform, filtering, and inverse Fourier transform, we obtained the results on the right. As can be seen, we successfully reduced noise area 1 in the narrowband band-stop filter noise filtering operation, and noise area 2 in the narrowband band-pass filter structure noise filtering. These results demonstrate the feasibility of this analysis approach and provide new insights for optimizing diverse photonic parameters.

The section that synergizes with percolation theory

In the methods of interaction between conventional photonics and different disciplines mentioned earlier, we convert the ordinary geometric parameters that characterize metasurface structure into probability distribution functions. The results obtained after processing with different methods usually require the setting of a threshold value to convert them into the original structural design parameters, "1" pixel or "0" pixel. However, the connection between the selection of different threshold values and the diversified performance of the device cannot be analyzed within the framework of conventional photonics theory. Here, by integrating percolation theory, we provide not only a qualitative theoretical analysis approach for threshold selection but also a solution to the common problem of abrupt performance changes caused by minor parameter alterations in photonic device design.

Percolation theory, as one of the fundamental concepts widely studied in statistical physics, probability theory and a scaling theory, is a phenomenological theory proposed to study critical phenomena based on summarizing, analyzing, and generalizing experimental results. Although the background knowledge of phase transitions has not been completely revealed, percolation theory can obtain percolation threshold p_c by analyzing experimental results according to its model characteristics, thereby identifying the phase transition point and the abrupt property changes it brings. The most classic two-dimensional model for percolation theory is a network model with n*n vertices, where adjacent vertices have a probability p of being connected, and whether each edge is connected is independent of each other. P corresponding to at least one path (percolation) traversing the entire network is the percolation threshold p_c. Such a model is called bond percolation, and our work mainly utilizes another type, site percolation (as shown in Figures 4A–4C). Unlike bond percolation, site percolation does not connect different vertices with probability p but occupies these vertices with probability p. Based on previous research, the percolation threshold obtained in this modeling method is approximately 0.593.[41–44]

We have conducted relevant calculations here, verifying percolation theory for both narrowband band-stop filters and narrowband band-stop filters. The probability of the pixel "1" appearing at each position in the overall sample is denoted as p. By changing pc, if p is less than p_c, it is recorded as 0; otherwise, it is recorded as 1. For the narrowband band-stop filter, it can be observed that when p_c is 0.5, the overall optical response abruptly changes from a disordered distribution to a trend with a certain narrowband band-stop effect. When p_c changes from 0.58 to 0.63, the device's transmission spectrum undergoes a significant change again (as shown in Figure 4D). The structure exhibits a more pronounced narrowband optical response effect, and the peak width is significantly narrower than the result at 0.5, further approaching the target optical response. A similar discovery can be made for the narrowband band-pass filter, where the narrowband band-pass transmission spectrum effect is significantly pronounced when the percolation threshold p_c is 0.57 (as shown in Figure 4E). However, after passing 0.593 and reaching 0.60, its transmission spectrum no longer exhibits a single-peak narrowband band-pass effect. From the previous results, it indicates that the modeling and analysis approach is quite consistent with the site percolation in percolation theory, and the percolation thresholds p_c of the device are basically around 0.59. Furthermore, the acquisition of the percolation threshold relies primarily on statistical analysis. As more related sample data are obtained in the future, the abrupt threshold p_c conforming to photonic devices can be calculated with greater accuracy.

DISCUSSION

In summary, our work integrates conventional photonics with expertise from seven distinct fields, including artificial intelligence, image denoising, multi-agent modeling of Physarum polycephalum, percolation theory, WFC algorithms, conventional electromagnetics, and

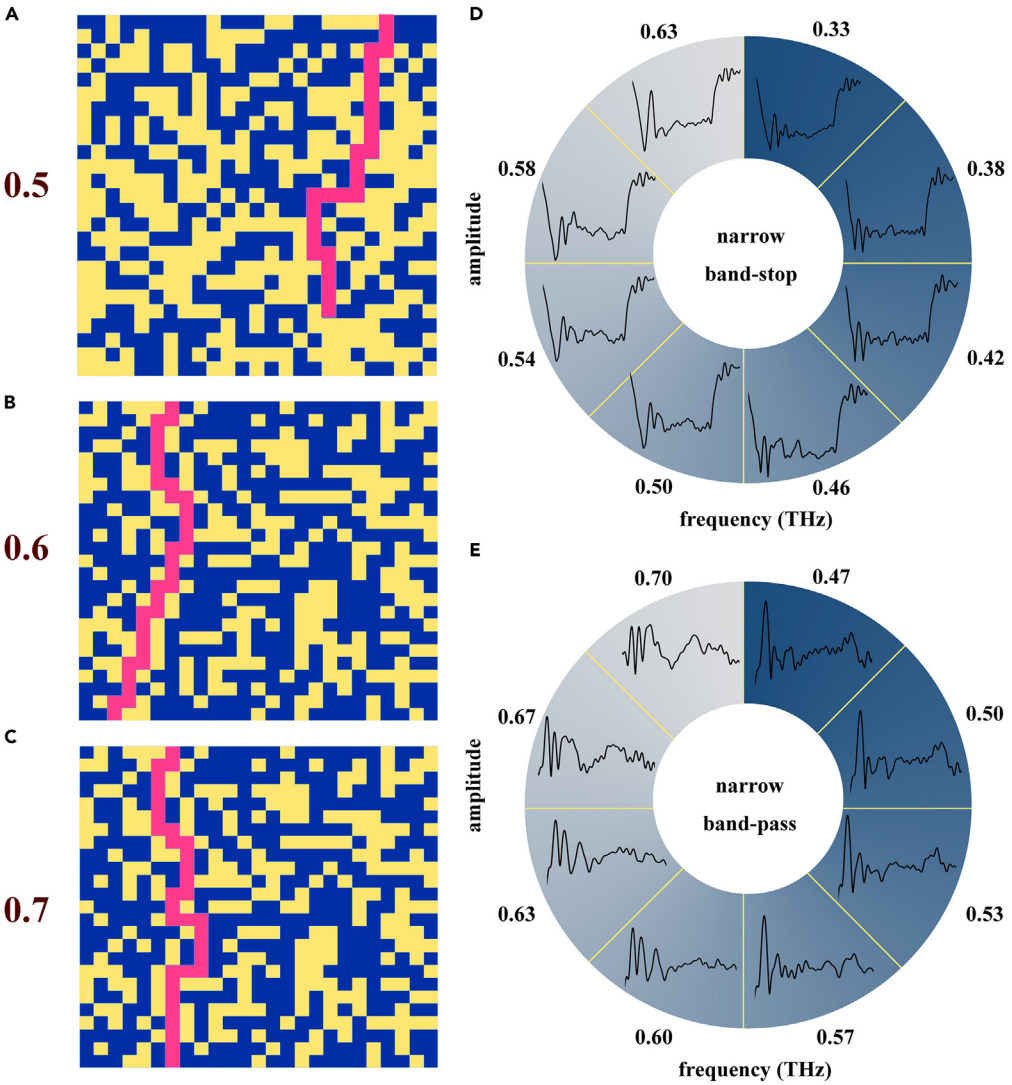

Figure 4. The results integration with percolation theory

(A–C) Schematic of percolation effect for different values of *p* in the structure model.

(D and E) Schematic of spectral changes in narrow band-stop and narrow band-pass under different threshold values of *p*.

mathematical model analysis. Simple geometric parameters within traditional theoretical frameworks have evolved into a variety of modeling approaches, such as pixel points, probability distributions, biological pathways, and noise areas, substantially increasing the diversity of photonic device design methodologies. Furthermore, after numerous theoretical and simulation validations, our results exhibit a high degree of congruence with the anticipated outcomes. Our study showcases the potential of "artificial intelligence science", thus providing additional design references for overcoming traditional barriers to interdisciplinary applications and facilitating further advancements in the realm of "AI for Science" and "Science for AI".

Limitations of the study

Our research is only focused on providing diversified analysis and optimization solutions for digital optical devices. The manuscript does not address the parallel optimization of interdisciplinary knowledge and the further enhancement of different device performances, which will require continuous exploration in future studies. Existing conventional photonics devices can only achieve improved optical performance by scanning parameters of specific geometric patterns, such as length, width, height, and angles. Currently, there are hardly any available means for optimization and analysis of new digital photonics devices or digital optical systems within the existing analytical framework. Supplementing new digital optical systems within the existing physical background, as proposed by the concept of meta-photonics, is crucial for establishing datasets and combining them with artificial intelligence techniques to enable deeper and transferable data analysis. Additionally,

it is essential to break the constraints of empirical knowledge in traditional designs and introduce new analytical perspectives. Although our work effectively utilizes GAN networks for data augmentation, the volume of data remain limited. We believe that the involvement of more research teams in advancing digital photonics and the availability of richer and more diverse data will facilitate the analysis of complex and outstanding optical problems.

STAR★METHODS

Detailed methods are provided in the online version of this paper and include the following:

- KEY RESOURCES TABLE
- RESOURCE AVAILABILITY
  - Lead contact
  - Materials availability
  - Data and code availability
- EXPERIMENTAL MODEL AND STUDY PARTICIPANT DETAILS
  - Experimental methods
- METHOD DETAILS
  - Model parameters and devices

SUPPLEMENTAL INFORMATION

Supplemental information can be found online at https://doi.org/10.1016/j.isci.2024.109838.

ACKNOWLEDGMENTS

The authors thank Dr. Weili Zhang, Dr. Chunmei Ouyang, Dr. Zhen Tian, Dr. Zhiyong Wang, Dr. Pengfei Zhu, Mrs Jing Huang and Dr. Tianjiao Zhao for the help in this work. The authors acknowledge the financial support from the National Key Research and Development Program of China (Grant No. 2022YFA1203502), and the National Natural Science Foundation of China (NSAF, No. U2230114).

AUTHOR CONTRIBUTIONS

Conceptualization, X.H.X. and L.W.; methodology, X.H.X., and Y.Q.R.; software, D.Z., X.H.X., Q.K.Z., and B.X.M.; writing- original draft, X.H.X. and Y.Q.R.; writing – review & editing, L.W.; supervision, D.Y.X. and J.Q.Y., visualization, X.H.X.; resources, X.H.X. and Y.Q.R.

DECLARATION OF INTERESTS

The authors declare no competing interests.

Received: February 16, 2024
Revised: April 16, 2024
Accepted: April 25, 2024
Published: April 27, 2024

REFERENCES

1. Chen, B., Huang, K., Raghupathi, S., Chandratreya, I., Du, Q., and Lipson, H. (2022). Automated discovery of fundamental variables hidden in experimental data. Nat. Comput. Sci. *2*, 433–442. https://doi.org/10.1038/s43588-022-00281-6.
2. Kramer, B. (2022). Learning state variables for physical systems. Nat. Comput. Sci. *2*, 414–415. https://doi.org/10.1038/s43588-022-00283-4.
3. Qian, C., Zheng, B., Shen, Y., Jing, L., Li, E., Shen, L., and Chen, H. (2020). Deep-learning-enabled self-adaptive microwave cloak without human intervention. Nat. Photonics *14*, 383–390. https://doi.org/10.1038/s41566-020-0604-2.
4. Zhu, R., Qiu, T., Wang, J., Sui, S., Hao, C., Liu, T., Li, Y., Feng, M., Zhang, A., Qiu, C.W., and Qu, S. (2021). Phase-to-pattern inverse design paradigm for fast realization of functional metasurfaces via transfer learning. Nat. Commun. *12*, 2974. https://doi.org/10.1038/s41467-021-23087-y.
5. Shi, L., Li, B., Kim, C., Kellnhofer, P., and Matusik, W. (2021). Author correction: Towards real-time photorealistic 3D holography with deep neural networks. Nature *593*, E13. https://doi.org/10.1038/s41586-021-03476-5.
6. Malkiel, I., Mrejen, M., Nagler, A., Arieli, U., Wolf, L., and Suchowski, H. (2018). Plasmonic nanostructure design and characterization via Deep Learning. Light Sci. Appl. *7*, 60. https://doi.org/10.1038/s41377-018-0060-7.
7. An, S., Zheng, B., Tang, H., Shalaginov, M.Y., Zhou, L., Li, H., Kang, M., Richardson, K.A., Gu, T., Hu, J., et al. (2021). Multifunctional metasurface design with a generative adversarial network. Adv. Opt. Mater. *9*, 2001433. https://doi.org/10.1002/adom.202001433.
8. Wu, C., Yu, H., Lee, S., Peng, R., Takeuchi, I., and Li, M. (2021). Programmable phase-change metasurfaces on waveguides for multimode photonic convolutional neural network. Nat. Commun. *12*, 96. https://doi.org/10.1038/s41467-020-20365-z.
9. Yang, B., Ma, D., Liu, W., Choi, D.Y., Li, Z., Cheng, H., Tian, J., and Chen, S. (2022). Deep-learning-based colorimetric polarization-angle detection with metasurfaces. Optica *9*, 217–220. https://doi.org/10.1364/OPTICA.449893.
10. Ma, W., Liu, Z., Kudyshev, Z.A., Boltasseva, A., Cai, W., and Liu, Y. (2021). Deep learning for the design of photonic structures. Nat. Photonics *15*, 77–90. https://doi.org/10.1038/s41566-020-0685-y.
11. Liu, Z., Zhu, D., Lee, K.T., Kim, A.S., Raju, L., and Cai, W. (2020). Compounding meta-atoms into metamolecules with hybrid artificial intelligence techniques. Adv. Mater. *32*, 1904790. https://doi.org/10.1002/adma.201904790.

12. Shaltout, A.M., Lagoudakis, K.G., van de Groep, J., Kim, S.J., Vučković, J., Shalaev, V.M., and Brongersma, M.L. (2019). Spatiotemporal light control with frequency-gradient metasurfaces. Science *365*, 374–377.
13. Han, Z., Ohno, S., and Minamide, H. (2020). Spectral phase singularity in a transmission-type double-layer metamaterial. Optica *7*, 1721–1728. https://doi.org/10.1364/OPTICA.404090.
14. Chen, C., Kaj, K., Zhao, X., Huang, Y., Averitt, R.D., and Zhang, X. (2022). On-demand terahertz surface wave generation with microelectromechanical-system-based metasurface. Optica *9*, 17–25. https://doi.org/10.1364/OPTICA.444999.
15. Zhao, X., Schalch, J., Zhang, J., Seren, H.R., Duan, G., Averitt, R.D., and Zhang, X. (2018). Electromechanically tunable metasurface transmission waveplate at terahertz frequencies. Optica *5*, 303–310. https://doi.org/10.1364/OPTICA.5.000303.
16. Kim, J., Seong, J., Yang, Y., Moon, S.W., Badloe, T., and Rho, J. (2022). Tunable metasurfaces towards versatile metalenses and metaholograms: a review. Adv. Photonics *4*, 024001. https://doi.org/10.1117/1.AP.4.2.024001.
17. Aieta, F., Genevet, P., Kats, M.A., Yu, N., Blanchard, R., Gaburro, Z., and Capasso, F. (2012). Aberration-free ultrathin flat lenses and axicons at telecom wavelengths based on plasmonic metasurfaces. Nano Lett. *12*, 4932–4936. https://doi.org/10.1021/nl302516v.
18. Zuo, C., Qian, J., Feng, S., Yin, W., Li, Y., Fan, P., Han, J., Qian, K., and Chen, Q. (2022). Deep learning in Optical metrology: a review. Light Sci. Appl. *11*, 39. https://doi.org/10.1038/s41377-022-00714-x.
19. Zhang, H., Gu, M., Jiang, X.D., Thompson, J., Cai, H., Paesani, S., Santagati, R., Laing, A., Zhang, Y., Yung, M.H., et al. (2021). An optical neural chip for implementing complex-valued neural network. Nat. Commun. *12*, 457. https://doi.org/10.1038/s41467-020-20719-7.
20. Zhu, H.H., Zou, J., Zhang, H., Shi, Y.Z., Luo, S.B., Wang, N., Cai, H., Wan, L.X., Wang, B., Jiang, X.D., et al. (2022). Space-efficient optical computing with an integrated chip diffractive neural network. Nat. Commun. *13*, 1044. https://doi.org/10.1038/s41467-022-28702-0.
21. Ashtiani, F., Geers, A.J., and Aflatouni, F. (2022). An on-chip photonic deep neural network for image classification. Nature *606*, 501–506. https://doi.org/10.1038/s41586-022-04714-0.
22. Shastri, B.J., Tait, A.N., Ferreira de Lima, T., Pernice, W.H.P., Bhaskaran, H., Wright, C.D., and Prucnal, P.R. (2021). Photonics for artificial intelligence and neuromorphic computing. Nat. Photonics *15*, 102–114. https://doi.org/10.1038/s41566-020-00754-y.
23. Mourgias-Alexandris, G., Moralis-Pegios, M., Tsakyridis, A., Simos, S., Dabos, G., Totovic, A., Passalis, N., Kirtas, M., Rutirawut, T., Gardes, F.Y., et al. (2022). Noise-resilient and high-speed deep learning with coherent silicon photonics. Nat. Commun. *13*, 5572. https://doi.org/10.1038/s41467-022-33259-z.
24. Bassi, A., Lochan, K., Satin, S., Singh, T.P., and Ulbricht, H. (2013). Models of wave-function collapse, underlying theories, and experimental tests. Rev. Mod. Phys. *85*, 471–527. https://doi.org/10.1103/RevModPhys.85.471.
25. Sun, C.P., Liu, X.F., Zhou, D.L., and Yu, S.X. (2000). Quantum measurement via Born-Oppenheimer adiabatic dynamics. Phys. Rev. A. *63*, 01211. https://doi.org/10.1103/PhysRevA.63.012111.
26. Ma, F., Lin, Y.S., Zhang, X., and Lee, C. (2014). Tunable multiband terahertz metamaterials using a reconfigurable electric split-ring resonator array. Light Sci. Appl. *3*, e171. https://doi.org/10.1038/lsa.2014.52.
27. Liu, P.Q., Luxmoore, I.J., Mikhailov, S.A., Savostianova, N.A., Valmorra, F., Faist, J., and Nash, G.R. (2015). Highly tunable hybrid metamaterials employing split-ring resonators strongly coupled to graphene surface plasmons. Nat. Commun. *6*, 8969. https://doi.org/10.1038/ncomms9969.
28. Husnik, M., Klein, M.W., Feth, N., König, M., Niegemann, J., Busch, K., Linden, S., and Wegener, M. (2008). Absolute extinction cross-section of individual magnetic split-ring resonators. Nat. Photonics *2*, 614–617. https://doi.org/10.1038/nphoton.2008.181.
29. Nakagaki, T., Yamada, H., and Tóth, A. (2000). Maze-solving by an amoeboid organism. Maze-solving by an amoeboid organism. Nature *407*, 470. https://doi.org/10.1038/35035159.
30. Nakagaki, T., Yamada, H., and Tóth, A. (2001). Path finding by tube morphogenesis in an amoeboid organism. Biophys. Chem. *92*, 47–52. https://doi.org/10.1016/s0301-4622(01)00179-x.
31. Tero, A., Kobayashi, R., and Nakagaki, T. (2007). A mathematical model for adaptive transport network in path finding by true slime mold. J. Theor. Biol. *244*, 553–564. https://doi.org/10.1016/j.jtbi.2006.07.015.
32. Nakagaki, T., Iima, M., Ueda, T., Nishiura, Y., Saigusa, T., Tero, A., Kobayashi, R., and Showalter, K. (2007). Minimum-risk path finding by an adaptive amoebal network. Phys. Rev. Lett. *99*, 068104. https://doi.org/10.1103/PhysRevLett.99.068104.
33. Tero, A., Takagi, S., Saigusa, T., Ito, K., Bebber, D.P., Fricker, M.D., Yumiki, K., Kobayashi, R., and Nakagaki, T. (2010). Rules for biologically inspired adaptive network design. Science *327*, 439–442. https://doi.org/10.1126/science.1177894.
34. Li, S., Chen, H., Wang, M., Heidari, A.A., and Mirjalili, S. (2020). Slime mould algorithm: A new method for stochastic optimization. Future Gener. Comp. Sy. *111*, 300–323. https://doi.org/10.1016/j.future.2020.03.055.
35. Kumar, C., Raj, T.D., Premkumar, M., and Raj, T.D. (2020). A new stochastic slime mould optimization algorithm for the estimation of solar photovoltaic cell parameters. Optik *223*, 165277. https://doi.org/10.1016/j.ijleo.2020.165277.
36. Burchett, J.N., Elek, O., Tejos, N., Prochaska, J.X., Tripp, T.M., Bordoloi, R., and Forbes, A.G. (2020). Revealing the dark threads of the cosmic web. Astrophys. J. Lett. *891*, L35. https://doi.org/10.3847/2041-8213/ab700c.
37. Zubaidi, S.L., Abdulkareem, I.H., Hashim, K.S., Al-Bugharbee, H., Ridha, H.M., Gharghan, S.K., Al-Qaim, F.F., Muradov, M., Kot, P., and Al-Khaddar, R. (2020). Hybridised artificial neural network model with slime mould algorithm: a novel methodology for prediction of urban stochastic water demand. Water *12*, 2692. https://doi.org/10.3390/w12102692.
38. Khan, T.M., Bailey, D.G., Khan, M.A.U., and Kong, Y. (2017). Efficient hardware implementation for fingerprint image enhancement using anisotropic gaussian filter. IEEE T Image Process *26*, 2116–2126. https://doi.org/10.1109/TIP.2017.2671781.
39. Mafi, M., Martin, H., Cabrerizo, M., Andrian, J., Barreto, A., and Adjouadi, M. (2019). A comprehensive survey on impulse and Gaussian denoising filters for digital images. Signal Process. *157*, 236–260. https://doi.org/10.1016/j.sigpro.2018.12.006.
40. Fu, H., Liu, W., Chen, H., and Wang, Z. (2020). An anisotropic Gaussian filtering model for image de-hazing. IEEE Access *8*, 175140–175149. https://doi.org/10.1109/ACCESS.2020.3026185.
41. Castin, Y., and Dum, R. (1996). Bose-einstein condensates in time dependent traps. Phys. Rev. Lett. *77*, 5315–5319. https://doi.org/10.1103/physrevlett.77.5315.
42. Huang, X., Yang, D., and Kang, Z. (2021). Impact of pore distribution characteristics on percolation threshold based on site percolation theory. Physica A *570*, 125800. https://doi.org/10.1016/j.physa.2021.125800.
43. Ottavi, H., and Gayda, J. (1973). Site percolation: Frontier curvature of clusters. J Phys *34*, 341–344. https://doi.org/10.1051/jphys:01973003405-6034100.
44. Haslegrave, J., and Panagiotis, C. (2021). Site percolation and isoperimetric inequalities for plane graphs. Random Struct Alg. *58*, 150–163. https://doi.org/10.1002/rsa.20946.

STAR★METHODS

KEY RESOURCES TABLE

REAGENT or RESOURCE	SOURCE	IDENTIFIER
Other		
THz-TDs System	Home-built	N/A
Software and algorithms		
CST Studio Suite	Electromagnetic Simulation software	https://www.3ds.com/products/simulia/cst-studio-suite

RESOURCE AVAILABILITY

Lead contact

Further information and requests for resources and information should be directed to and will be fulfilled by Liang Wu, (wuliang@tju.edu.cn).

Materials availability

This study did not generate new unique materials.

Data and code availability

- Data reported in this paper will be shared by the lead contact upon request.
- This paper dose not report original code.
- Any additional information required to reanalyze the data reported in this paper is available from the lead contact upon request.

EXPERIMENTAL MODEL AND STUDY PARTICIPANT DETAILS

Experimental methods

In the experiment, we selected the most representative structural patterns from each interdisciplinary design scheme in this study and used photolithography techniques to fabricate these devices. As shown in Figure S1, the first column shows the laser scanning confocal microscopy (LSCM) images of the devices, the second column shows the simulation results of the devices obtained by inverse design, and the third column shows the experiment results of the corresponding devices. Although the designed devices in this work originate from knowledge in different domains, they share a common structure of high-resistivity silicon substrate and aluminum structures of the same thickness (the thickness of the substrate is 500 μm, and the thickness of the aluminum part is 200 nm). Therefore, for experimental validation, we selected two devices to demonstrate their bandpass and bandstop functionalities, respectively. Figure S1A shows the bandpass structure obtained based on Physarum polycephalum, while Figure S1B depicts the bandpass structure 'scabbard' obtained through transfer learning from the ViT model. Figure S1C represents the bandstop structure 'shield' obtained through transfer learning. Figure S1D represents the bandstop structure 'analog clock' obtained through transfer learning. The selection of transfer learning patterns is mainly because, compared to other purely '01' pixelated structures, these patterns are closer to the intuitive understanding and analytical system of human perception of shapes. We aim to facilitate the emergence of new knowledge through an AI-based process. The pump source consisted of a femtosecond laser with a single pulse width of 26 fs, a repetition frequency of 88 MHz, and an average power of 10 mW. The emitter used was a low-temperature gallium arsenide antenna with a linewidth of 40 μm and a spacing of 120 μm. The receiver employed a sapphire-Si detector with a dipole separation of 5 and a dipole size of 20. During the measurement using the THz-TDs system, we observed significant fluctuations and instability in the THz wave energy at the 0–0.15 THz range. Therefore, we excluded this portion of the data. It can be seen that both the overall trend and peak positions exhibit a high level of agreement.

METHOD DETAILS

Model parameters and devices

Generative Adversarial Networks (GANs) were introduced in 2014, have achieved remarkable success in various fields such as image generation, speech synthesis, natural language processing. Through the adversarial training between the generator and the discriminator, the generator learns to generate more realistic samples, while the discriminator learns to better distinguish between real and generated samples. GANs employ a minimax objective function to train the generator and the discriminator:

$$\min_G \max_D V(D,G) = E_{x\sim Pdata(x)}[\log D(x)] + E_{z\sim p_z(z)}[\log(1 - D(G(z)))]$$

where G represents the generator, D represents the discriminator, x represents real data samples drawn from the true data distribution $p_{data}(x)$, z represents random noise samples drawn from a prior distribution $p_z(z)$, and $G(z)$ represents the generated samples from the generator network. $E_{x\sim p_{data}(x)}[\log D(x)]$ encourages the discriminator to correctly classify real data samples as $E_{z\sim p_z(z)}[\log(1 - D(G(z)))]$ encourages the discriminator to correctly classify generated samples as 0. The generator aims to minimize the second term to generate samples that can deceive the discriminator and be classified as real.

Through the iterative training process, the generator learns to generate more realistic samples that can better fool the discriminator, while the discriminator learns to better distinguish between real and generated samples.

Vision Transformer (ViT) is a neural network model that applies the Transformer architecture to the field of computer vision. It revolutionizes traditional approaches to image classification by treating images as sequences of tokens and leveraging self-attention mechanisms to capture global context information. The key idea of ViT is to divide an input image into a grid of patches, which are then reshaped and flattened into a sequence of tokens. Each token is linearly projected and embedded with positional encodings to retain spatial information. This sequence of tokens serves as the input of Transformer that consists of multiple layers of self-attention and feedforward neural networks.

The generator and discriminator in GAN are both composed of two layers of CNNs. The training dataset was trained for a total of 20 epochs. The batch size is 8 in all experiments. The optimizer we used is adam where learning rate is 1^{e-4}, β_1 is 0.9, β_2 is 0.999. The neural networks are constructed under the open-source machine learning framework of Pytorch. All experiments were executed on a single Nvidia a6000 GPU.